

Transport Properties and Solvation Structure of Mixtures of Carbon Dioxide and Room-Temperature Ionic Liquids

Masashi Demizu,[1] Masafumi Harada,[2] Kenji Saijo,[3] Masahide Terazima,[1] and Yoshifumi Kimura*[1]

[1]Department of Chemistry, Graduate School of Science, Kyoto University, Kyoto 606-8502

[2]Department of Health Science and Clothing Environment, Faculty of Human Life and Environment, Nara Women's University, Nara 630-8506

[3]Department of Polymer Chemistry, Graduate School of Engineering, Kyoto University, Kyoto 615-8510

Received July 16, 2010; E-mail: ykimura@kuchem.kyoto-u.ac.jp

Translational diffusion coefficients of diphenylcyclopropenone (DPCP), diphenylacetylene (DPA), and carbon monoxide (CO) in carbon dioxide (CO_2) mixtures of 1-butyl-3-methylimidazolium bis(trifluoromethanesulfonyl)amide ([BMIm][NTf_2]) and 1-butyl-3-methylimidazolium tetrafluoroborate ([BMIm][BF_4]), respectively, were determined by transient grating (TG) spectroscopy under various pressures of CO_2. With increasing CO_2 pressure up to 15 MPa, the diffusion coefficients of DPCP and DPA increased by an order of magnitude, while the increase of the diffusion coefficient of CO was relatively small. Sound velocities of the mixtures were also determined by TG spectroscopy, which decreased by ca. 20% with increasing pressure up to 10 MPa, and then turned to increase with pressure. The solvation structure around DPCP was also investigated by Raman spectroscopy. It was found that the vibrational spectra of solute and solvent molecules did not show remarkable changes. Small-angle X-ray scattering (SAXS) profiles for CO_2 mixture of 1-octyl-3-methylimidazolium tetrafluoroborate ([OMIm][BF_4]) were measured under various pressures of CO_2. The peak observed for the SAXS profile at 3 nm^{-1} for [OMIm][BF_4] did not show meaningful shift with increasing CO_2 pressure, while the peak width showed a small increase.

Some room-temperature ionic liquids (RTILs) are known to dissolve a significant amount of carbon dioxide,[1] and currently numerous studies are undertaken to apply the mixtures for the storage of CO_2 and/or the further synthesis of materials.[2] From a physicochemical point of view, the thermodynamic properties of the mixture are also quite interesting. For example, the expansion of the liquid phase by applying CO_2 pressure is small in comparison with conventional liquids.[3–5] According to molecular dynamics simulation of the mixture, CO_2 molecules were suggested to be dissolved into the "free volume" sites produced by the local structure of cation and anion.[6–8] Kanakubo et al. measured the radial distribution function of a mixture of CO_2 and 1-butyl-3-methylimidazolium hexafluorophosphate ([BMIm][PF_6]) by X-ray scattering, and obtained a structure similar to one predicted by MD simulations.[9] The MD simulations also suggested that CO_2 molecules more strongly interact with anions such as BF_4^- and PF_6^-.[6–8] IR and Raman spectroscopic studies also suggested stronger interaction of CO_2 with anion.[10–12] Seki et al. measured the ATR-IR spectrum of a mixture of several RTILs and CO_2, and found that the vibrational modes related to BF_4^- or PF_6^- anion show a small shift with increasing pressure, suggesting the interaction between CO_2 and anion.[11] However, the changes of the vibrational modes, especially for cation, were found to be small and the conformational structures of cation and anion were suggested to be almost conserved irrespective of the concentrations of CO_2.[11–13]

On the other hand, the dynamic properties of the mixture dramatically change with increasing CO_2 pressure. For example, Liu et al. have reported the viscosity of a CO_2 mixture of [BMIm][PF_6] system along a saturated line.[14] According to their study, the viscosity of the mixture dramatically decreases with increasing CO_2 pressure, and the variation is large in the lower pressure region at lower temperature. Kanakubo et al. reported the electric conductivity of a CO_2 mixture of [BMIm][PF_6][15] and found a more enhanced effect of CO_2 on the conductivity than on the viscosity reported by Liu et al. Demizu et al. have reported the translational diffusion coefficients of solute molecules dissolved in a CO_2 mixture of [BMIm][PF_6].[16] They found that the diffusion coefficients of the solutes dissolved in the mixture remarkably increase with increasing CO_2 pressure, and that those of the larger molecules are more remarkably dependent on the pressure. Recent MD simulations of [BMIm][PF_6] with different compositions of CO_2 also indicated that the diffusion coefficients of cation, anion, and CO_2 increase by an order of magnitude with increasing the concentration of CO_2 to 70 mol %, and the dependence is more significant for cation and anion than CO_2.[17] These observations suggest that the dynamic properties are significantly affected by CO_2, while the variation of the static structure is small.

In this paper, we will present the results of a further transient grating (TG) study of mixtures of CO_2 and other RTILs, 1-butyl-3-methylimidazolium bis(trifluoromethanesulfonyl)amide ([BMIm][NTf_2]) and 1-butyl-3-methylimidazolium tetrafluoro-

Published on the web January 1, 2011; doi:10.1246/bcsj.20100202

borate ([BMIm][BF_4]), together with a study of the CO_2 effect on solvation structure and nanoscale ordering. By TG, we can determine the sound velocity of the mixtures and the diffusion coefficients of the solute molecules dissolved in the mixture. We utilized the photodissociation reaction of diphenylcyclopropenone (DPCP) into diphenylacetylene (DPA) and carbon monoxide (CO), and determined the sound velocity and the translational diffusion coefficients of CO, DPA, and DPCP in CO_2 mixtures of [BMIm][NTf_2] and [BMIm][BF_4], respectively. We found significant dependence of these properties on the CO_2 pressure. In order to discuss the observed dynamics in relation with the solvation structure and structure change of the CO_2 mixtures of RTILs, we have also performed Raman spectroscopic measurement to obtain the local structure information around the solute molecule, and small-angle X-ray scattering (SAXS) measurement to obtain the larger-scale structure information. Previously Fujisawa et al. have indicated that the Raman band around 1625 cm^{-1} of DPCP assigned to the C=O + C=C stretching vibration is a good indicator of Lewis acidity of the solvent.[18] By measuring Raman spectra of the DPCP solution of the mixture, we tried to extract how the local environment around DPCP will change with CO_2 pressure. Although Raman spectra reflect the change of the local structure of RTILs, it is insensitive to the larger size domain structure which was proposed for RTILs.[19–25] For example, Triolo et al. measured small-angle X-ray scattering intensity for imidazolium-based ionic liquids with different lengths of alkyl side chains.[26] They found that there appears a peak in a few nm^{-1} region for RTILs with longer alkyl chains (greater than C_6), and that the peak position depends on the alkyl chain length of the imidazolium cation. They attributed this interference peak to alkyl chain segregation in RTILs by referring to a report by Canongia Lopes and Pádua, which proposed the occurrence of alkyl chain segregation from MD simulation.[24] Similar results are reported for RTILs other than the imidazolium-cation based ones,[27] and hence this nanoscale ordering is thought to be a common nature of RTILs with a long alkyl chain. Although the segregated structure is not observed for BMIm-cation-based ionic liquids used for the study of the present TG spectroscopy, it is quite an interesting issue how this peak will be affected by the presence of CO_2, and useful information will be extracted from the study.

In the following section, the experimental methods used in this paper and some details of the analysis of the TG signal will be given. Then, the results of the sound velocity and the diffusion coefficients will be presented. These values are discussed in relation with the solvation structure and nanoscale ordering measured by the Raman spectroscopy and the SAXS.

Experimental

Materials. [BMIm][NTf_2] and [BMIm][BF_4] were purchased from Kanto Kagaku. 1-Octyl-3-methylimidazolium tetrafluoroborate ([OMIm][BF_4]) was purchased from Merck. DPCP (Nacalai Tesque) was used after recrystallization from ethanol. CO_2 (>99.99%) supplied by Ekika Tansan Co. and Showa Tansan Co. was used without further purification.

TG Measurement. In TG spectroscopy, two laser pulses are introduced into a sample solution simultaneously, which make a transient optical grating in the solution. If photoreactive molecules are dissolved in the solution, the molecules are photoexcited at the bright fringe of the optical grating which causes heat expansion of the solution and/or a variation of molecular species. The grating disappears due to the thermal diffusion and molecular diffusion. These processes can be monitored by the intensity of the diffracted light of the probe beam incident on the grating.

Experimental setups for the TG measurement under high-pressure CO_2 are described elsewhere.[16] Briefly, the 355 nm (λ_{pump}) third harmonic of a Nd:YAG laser (Continuum, Minilite II) was used as an excitation pulse, and a 633 nm He-Ne laser beam (Lasos Lasertechnik, LGK7654-8) was used as a probe beam. The TG signal was detected by a photomultiplier tube (Hamamatsu photonics, R3896) and averaged by a digital oscilloscope (Tektronix, DPO7104). In the measurements, we used the high-pressure optical cell[28] which had a larger inner bottom area to use a larger magnetic stirrer than the one in the previous report[16] in order to improve the efficiency of the CO_2 dissolution. The inner volume of the cell was ca. 10 cm^3. The temperature of the cell was controlled by circulating thermostated water through the water pass through the cell.

For the TG measurement, DPCP solution of RTIL was filtered through a membrane filter in order to remove undissolved solute and/or fine dust. The optical density of the sample solution was adjusted to be around 1 for 1 cm optical path length at 355 nm (the concentration of DPCP was ca. 2 mM). After evacuation under a vacuum pump for more than 3 h at 60 °C, the sample solution was placed into the high-pressure cell, and then the cell was sealed. CO_2 supplied from a bomb was compressed by a high-pressure pump (Jasco SCF-Get). After equilibration of the temperature of the cell (40.0 °C), CO_2 was introduced. The solution was vigorously stirred by a magnetic stirrer. After equilibrium was attained (more than 3 h), the TG measurement was performed at each CO_2 pressure. The pressure of the system was monitored by a strain gauge (Kyowa PGM-500KH). The equilibration was tested by the stability of the pressure. The time required to attain equilibrium was also confirmed by the Raman intensity of CO_2. After the experiment, the viscosity of the sample was measured at 25 °C using a viscometer (Brookfield LVDV-II, cone plate CPE-40). The value was 50 and 96 mPa s for [BMIm][NTf_2] and [BMIm][BF_4], respectively, which were close to the reported values.[29]

Since the TG signals in the CO_2 mixtures of [BMIm][NTf_2] and [BMIm][BF_4] were similar to those observed in the CO_2 mixture of [BMIm][PF_6], we analyzed the signals in similar ways described in previous papers.[16,30] Briefly, in the initial several hundred nanoseconds, an oscillation signal due to the acoustic wave was detected. From the oscillation frequency (ω) of the signal, the sound velocity (c) of the mixture was determined by using the relation of $c = (\omega/q)$ (eq 1 in Ref. 16), where q is the grating lattice vector determined by $q = 4\pi \sin(\theta/2)/\lambda_{pump}$ (θ crossing angle between pump pulses). After dumping the acoustic signal, the thermal grating signal decayed in the microsecond time range, and the thermal diffusivity of the mixture (D_{th}) was determined by fitting the decay to a square of an exponential function with a constant offset. After the decay of thermal grating signals, the diffusion

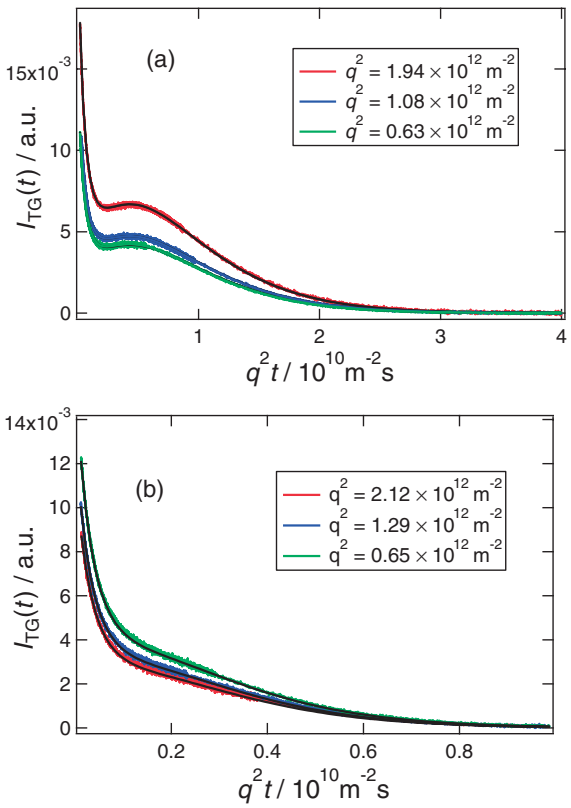

Figure 1. Typical example of TG signal for the diffusion of CO, DPA, and DPCP in [BMIm][NTf_2] at (a) 3 and (b) 10 MPa of CO_2 and different q-values.

signals due to CO, DPA, and DPCP were detected over ms time range. Typical examples of the TG signals for diffusion in a CO_2 mixture of [BMIm][NTf_2] are shown in Figure 1. In the figure, the horizontal scale is q^2t. The signal was simulated by a square of the sum of three exponential decays, each of which corresponds to the diffusion of CO, DPA, and DPCP, respectively, as

$$I_{TG}(t) \propto (\Delta n_{CO} \exp(-D_{CO}q^2t) + \Delta n_{DPA} \exp(-D_{DPA}q^2t) - \Delta n_{DPCP} \exp(-D_{DPCP}q^2t))^2 \quad (1)$$

where Δn_{CO}, Δn_{DPA}, and Δn_{DPCP}, are the initial peak null differences of the refractive indexes produced by the species gratings. D_{CO}, D_{DPA}, and D_{DPCP} are the translational diffusion coefficients. As was done previously,[30] in the fitting we fixed the ratio of Δn_{DPCP} to Δn_{DPA} ($\Delta n_{DPCP}/\Delta n_{DPA} = 1.15$) in order to improve the fitting reliability. In the present work, we have also assumed that the ratio of Δn_{CO} and Δn_{DPA} is constant irrespective of the CO_2 pressure, since at higher CO_2 pressure the diffusion coefficients became close to one another and the separation of three components was difficult as is shown in Figure 1b. We have determined the ratio ($\Delta n_{DPA}/\Delta n_{CO}$) from the signal at 0.1 MPa as -3.60 and -4.33 for the CO_2 mixtures of [BMIm][NTf_2] and [BMIm][BF_4], respectively. The diffusion coefficients of CO, DPA, and DPCP were determined by fitting the time profiles at different q-values simultaneously as is shown by the solid lines in Figure 1. We have also re-analyzed the data for the CO_2 mixture of [BMIm][PF_6] by fixing the ratio $\Delta n_{DPA}/\Delta n_{CO}$ as -5.40. The diffusion coefficients of DPA and DPCP in [BMIm][PF_6] were almost unchanged from the reported values previously,[16] although the diffusion coefficients of CO at higher CO_2 pressures were somewhat (ca. 10%) modified.

Raman Measurement. Raman spectrum of the mixture was measured in a back scattering geometry using an electronically cooled CCD camera (Princeton Instruments; Spec-10:400BRXTE) attached to a 64 cm monochromator (Jobin Yvon; T64000) with 1800 and 600 lines mm^{-1} gratings as described elsewhere.[31] A 514.5 nm laser line of Ar^+ laser (Coherent: Enterprise) was used for the Raman probe. The sample solutions were prepared in the same way described in the section of TG measurement. The concentration of DPCP was ca. 25 mM. After the equilibrium was attained at 40.0 °C, the Raman measurements were performed at each CO_2 pressure.

SAXS Measurement. Small-angle X-ray scattering (SAXS) experiments were performed at BL-15A station in High Energy Accelerator Research Organization-Photon Factory (KEK-PF). X-ray beam of 1.5 Å in wavelength was selected and injected into a high-pressure cell. Scattering data were collected by a position sensitive proportional counter (PSPC). The cell we used in the SAXS measurements is described elsewhere,[32] and it was quite similar to the one used in the TG measurement except that the cell had two diamond windows in the opposite sides and that the optical path length was about 1 mm. In the measurement, RTIL was poured into the cell and the high-pressure cell was closed at first. Then CO_2 was introduced into the cell. The solution was vigorously stirred by a magnetic stirrer within the cell. After equilibrium was attained at 40.0 °C, the high-pressure cell was placed in the beam line, and the SAXS measurement was performed. After measurement at one CO_2 pressure, the cell was moved off line in order to apply higher CO_2 pressure, and then the scattering intensity at the higher pressure was measured after equilibrium was attained. The scattering intensities at each pressure were corrected by the absorption of the X-ray in the sample, and plotted as a function of the scattering vector q_{SAX} defined as $q_{SAX} = (4\pi \sin(\theta/2))/\lambda_{X\text{-ray}}$, in which θ is the scattering angle and $\lambda_{X\text{-ray}}$ the wavelength.

Results and Discussion

Sound Velocity and Isentropic Compressibility. Tables 1 and 2 summarize the results of the sound velocities of the CO_2 mixtures of [BMIm][NTf_2] and [BMIm][BF_4] under different pressures, respectively. The sound velocities at 0.1 MPa determined here (1206 m s^{-1} for [BMIm][NTf_2] and 1524 m s^{-1} for [BMIm][BF_4]) are slightly larger than the values reported in the literature measured at a sound frequency of 0.5 MHz (1194.5 and 1503.36 m s^{-1}, respectively).[33,34] This is the same tendency as our previous report for [BMIm][PF_6],[16] and we consider that the slight difference from the reported value may be due to the sound velocity dispersion of RTILs,[35] since our sound velocity is determined at somewhat higher frequency (ca. 30 MHz). Figure 2 shows the pressure dependence of the sound velocity against the CO_2 pressure, together with the results for [BMIm][PF_6] previously reported.[16] As in the case of [BMIm][PF_6], the sound velocity decreases with increasing CO_2 pressure to nearly 10.0 MPa in

Table 1. Sound Velocity (c), Calculated Values of Mole Fraction of CO_2 (X_{CO_2}), Density of Liquid Phase (ρ), and Isentropic Compressibility β_S under Different Pressures of CO_2 for [BMIm][NTf_2] at 313 K

P/MPa	c/m s^{-1} a)	X_{CO_2} b)	ρ/g cm^{-3} c)	β_S/GPa^{-1} d)
0.1	1206	0	1.46	0.472
2.0	1165	0.31	1.43	0.517
4.0	1111	0.50	1.40	0.578
6.0	1059	0.62	1.39	0.643
8.0	1008	0.69	1.38	0.712
10.0	994	0.73	1.38	0.731
12.0	995	0.75	1.39	0.728
14.0	995	0.77	1.39	0.724
16.0	999	—e)	—e)	—e)
17.0	1000	—e)	—e)	—e)
19.1	1005	—e)	—e)	—e)

a) The error of the sound velocity is estimated as ±0.5% of the value. b) Estimated from the data in Ref. 5. c) Estimated from the X_{CO_2} and the relation between $\Delta V/V$ of eq 4 in Ref. 5. d) Calculated from eq 2. e) Data are not available.

Table 2. Sound Velocity (c), Calculated Values of Mole Fraction of CO_2 (X_{CO_2}), Density of Liquid Phase (ρ), and Isentropic Compressibility β_S under Different Pressures of CO_2 for [BMIm][BF_4] at 313 K

P/MPa	c/m s^{-1} a)	X_{CO_2} b)	ρ/g cm^{-3} c)	β_S/GPa^{-1} d)
0.1	1524	0	1.17	0.368
2.0	1477	0.20	1.18	0.388
4.0	1426	0.34	1.18	0.417
6.0	1372	0.43	1.18	0.452
8.0	1335	0.51	1.19	0.473
10.0	1324	—e)	—e)	—e)
15.0	1326	—e)	—e)	—e)
20.0	1332	—e)	—e)	—e)

a) The error of the sound velocity is estimated as ±0.5% of the value. b) Estimated from the data in Ref. 5. c) Estimated from the X_{CO_2} and the relation between $\Delta V/V$ of eq 4 in Ref. 5. d) Calculated from eq 2. e) Data are not available.

contrast to the case when the static pressure is applied to RTILs.[33] Above 10 MPa, the dependence becomes quite small, and it shows the tendency to be larger again. The sound velocity in the low-frequency limit is related to the isentropic compressibility β_S as

$$\beta_s = \frac{1}{\rho}\left(\frac{\partial \rho}{\partial P}\right)_S = \frac{1}{\rho c^2} \quad (2)$$

Using available information on the density of liquid phase (ρ) and the sound velocity (c), the value of β_S was calculated as is reported previously in the following manner.[16] According to Ref. 5, the system volume change with pressure ($\Delta V/V$) defined by eq 4.4 of Ref. 5 is correlated with the mole fraction of CO_2 (X_{CO_2}) in the liquid phase. Using the data in the supporting information (Table SI7 for [BMIm][NTf_2], Table SI2 for [BMIm][BF_4]) in Ref. 5, we have fitted $\Delta V/V$ to a third polynomial function of X_{CO_2}, and estimated the density of the liquid phase (ρ) as a function of X_{CO_2}. The value of X_{CO_2} at each CO_2 pressure was also estimated by interpolating

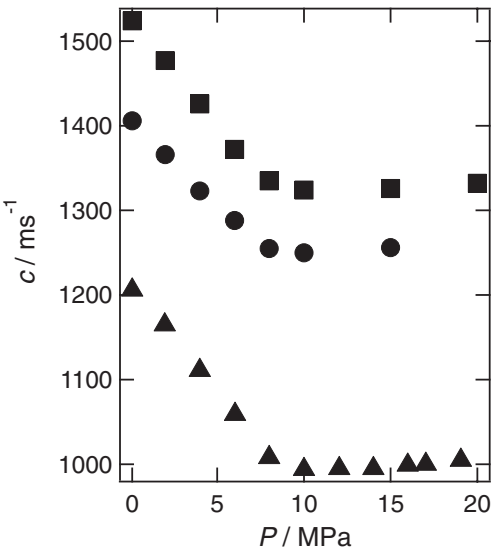

Figure 2. CO_2 pressure dependence of the sound velocity of mixtures of CO_2 and RTILs (●: [BMIm][PF_6] from Ref. 16, ▲: [BMIm][NTf_2], and ■: [BMIm][BF_4]).

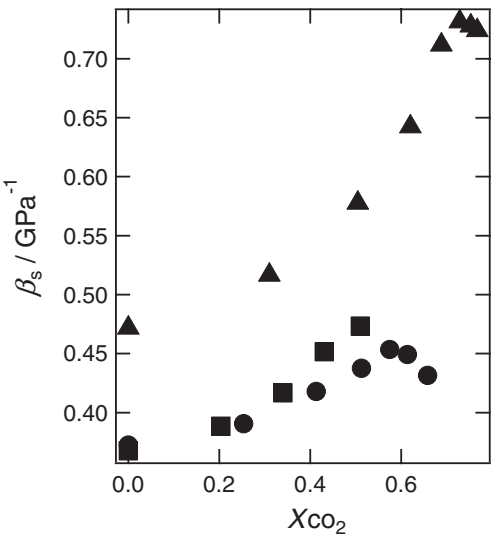

Figure 3. Dependence of the isentropic compressibility of mixtures of CO_2 and RTILs on the mole fraction of CO_2 in the solution (●: [BMIm][PF_6] from Ref. 16, ▲: [BMIm][NTf_2], and ■: [BMIm][BF_4]).

the data in Ref. 5. In the calculation we neglected the sound velocity dispersion.

The values of X_{CO_2}, ρ, and β_S thus calculated are summarized in Tables 1 and 2. The values of β_S are plotted against X_{CO_2} in Figure 3. The dependence of β_S on the pressure for CO_2 mixtures of [BMIm][NTf_2] and [BMIm][BF_4] are quite similar to that for a CO_2 mixture of [BMIm][PF_6]; i.e., the dissolution of CO_2 makes the isentropic compressibility of RTILs larger up to near the saturation pressure. Since the isentropic compressibility is proportional to the isothermal compressibility, an increase of the density fluctuation increases β_S. As mentioned in previous work,[16] the variation of the compressibility will be explained by the way of CO_2 dissolution predicted by the MD simulation. According to

Table 3. Thermal Diffusivity and Translational Diffusion Coefficients of CO, DPA, and DPCP in a Mixture of CO_2 and [BMIm][NTf_2] under Different Pressures of CO_2 at 313 K

P/MPa	X_{CO_2} [a]	V_r [b]	D_{th} /10^{-8} m^2 s^{-1}	D_{CO} /10^{-10} m^2 s^{-1}	D_{DPA} /10^{-11} m^2 s^{-1}	D_{DPCP} /10^{-11} m^2 s^{-1}
0.1	0	1	6.13 ± 0.08	7.51 ± 0.1	6.96 ± 0.3	4.41 ± 0.3
1.0	0.17	1.03	6.22 ± 0.05	9.67 ± 0.3	10.4 ± 0.5	6.64 ± 0.4
2.0	0.31	1.07	6.08 ± 0.07	12.2 ± 0.6	14.6 ± 0.6	9.59 ± 0.6
3.0	0.42	1.11	6.12 ± 0.05	13.8 ± 0.3	17.7 ± 0.3	11.8 ± 0.2
4.0	0.50	1.15	6.08 ± 0.07	16.4 ± 0.2	22.8 ± 0.4	15.5 ± 0.2
5.0	0.57	1.19	5.98 ± 0.08	18.0 ± 0.2	27.5 ± 0.4	19.0 ± 0.4
6.0	0.62	1.23	5.97 ± 0.05	19.0 ± 0.6	31.7 ± 0.6	22.3 ± 0.6
8.0	0.69	1.30	6.18 ± 0.05	21.3 ± 0.5	42.7 ± 0.6	31.0 ± 0.5
10.0	0.73	1.35	6.01 ± 0.18	21.6 ± 0.3	48.2 ± 0.7	35.2 ± 0.6
12.0	0.75	1.39	5.94 ± 0.17	21.7 ± 0.5	49.1 ± 1.8	35.8 ± 1.4
14.0	0.77	1.42	5.99 ± 0.26	21.6 ± 0.5	50.5 ± 0.4	36.7 ± 0.2

a) Estimated from the data in Ref. 5. b) Estimated from the X_{CO_2} and the relation between $\Delta V/V$ of eq 4 in Ref. 5.

Table 4. Thermal Diffusivity and Translational Diffusion Coefficients of CO, DPA, and DPCP in a Mixture of CO_2 and [BMIm][BF_4] under Different Pressures of CO_2 at 313 K

P/MPa	X_{CO_2} [a]	V_r [b]	D_{th} /10^{-8} m^2 s^{-1}	D_{CO} /10^{-10} m^2 s^{-1}	D_{DPA} /10^{-11} m^2 s^{-1}	D_{DPCP} /10^{-11} m^2 s^{-1}
0.1	0	1	9.03 ± 0.22	4.77 ± 0.1	4.66 ± 0.1	2.82 ± 0.1
2.0	0.20	1.04	9.25 ± 0.10	7.14 ± 0.3	8.48 ± 0.2	5.53 ± 0.4
4.0	0.34	1.09	9.02 ± 0.09	9.26 ± 0.4	13.5 ± 0.6	8.87 ± 0.6
6.0	0.43	1.14	8.93 ± 0.09	11.0 ± 0.4	18.0 ± 0.4	12.0 ± 0.2
8.0	0.51	1.19	8.96 ± 0.08	11.6 ± 0.9	22.0 ± 1.7	14.7 ± 0.5
10.0	—[c]	—[c]	9.11 ± 0.17	11.8 ± 0.6	23.1 ± 1.0	15.8 ± 0.9
15.0	—[c]	—[c]	9.04 ± 0.11	12.4 ± 0.3	25.8 ± 0.8	17.8 ± 0.9

a) Estimated from the data in Ref. 5. b) Estimated from the X_{CO_2} and the relation between $\Delta V/V$ of eq 4 in Ref. 5. c) Data are not available.

Table 5. Translational Diffusion Coefficients of CO, DPA, and DPCP in a Mixture of CO_2 and [BMIm][PF_6] under Different Pressures of CO_2 at 313 K

P/MPa	X_{CO_2} [a]	V_r [b]	D_{CO} /10^{-10} m^2 s^{-1}	D_{DPA} /10^{-11} m^2 s^{-1}	D_{DPCP} /10^{-11} m^2 s^{-1}
0.1	0	1	3.80 ± 0.1	2.12 ± 0.2	1.25 ± 0.1
1.0	0.14	1.01	5.43 ± 0.1	3.82 ± 0.1	2.48 ± 0.2
2.0	0.25	1.04	6.62 ± 1.0	5.62 ± 0.6	3.46 ± 0.5
3.0	0.34	1.07	8.00 ± 0.8	7.54 ± 0.3	4.69 ± 0.4
4.0	0.41	1.10	9.32 ± 0.2	9.64 ± 0.2	6.14 ± 0.3
6.0	0.51	1.15	10.8 ± 0.7	13.9 ± 0.2	9.04 ± 0.2
8.0	0.57	1.17	13.6 ± 0.5	20.2 ± 0.8	13.4 ± 0.5
10.0	0.61	1.19	13.8 ± 0.7	21.2 ± 1.1	14.2 ± 0.8
15.0	0.66	1.20	13.8 ± 0.4	22.6 ± 0.7	15.1 ± 0.5

a) Estimated from the data in Ref. 5. b) Estimated from the X_{CO_2} and the relation between $\Delta V/V$ of eq 4 in Ref. 5.

MD simulations of CO_2 dissolved in [BMIm][PF_6], CO_2 molecules are suggested to be localized around the sites of PF_6 anion.[7,17] By the occupation of CO_2 on specific sites in RTILs, the interaction between cation and anion may become loose due to the shielding effect of Coulombic interaction. As a result, the mean distance between ions becomes large as is represented by the occupation volume of ions. In Tables 3–5, we show the relative volume expansion of the mixture, V_r, which is defined as the ratio of the volume of the CO_2 mixture with 1 molar RTIL to the molar volume of pure RTIL. These values were calculated using the data in Ref. 5. As shown in Tables, V_r increases with increasing X_{CO_2}, suggesting that the ion concentration per unit volume becomes small. Therefore it is reasonable that the density fluctuation increases with increasing the CO_2 pressure.

It is noteworthy that the effect of CO_2 is more remarkable for [BMIm][NTf_2] than for [BMIm][PF_6] and [BMIm][BF_4]. It is reported that there exist two conformers of NTf_2^- anion (s-cis and s-trans conformers), and that they are in conformational equilibrium in RTILs.[36] Due to the shielding effect of the Coulomb force by CO_2, the conformation equilibrium is expected to change, which may result in the enhancement of

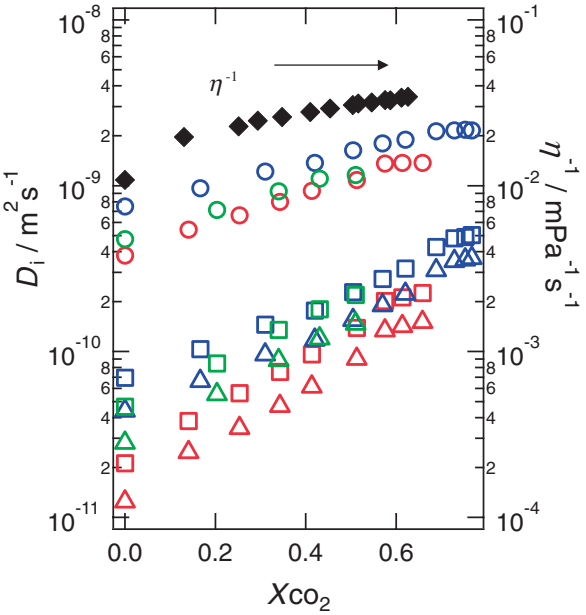

Figure 4. Dependence of translational diffusion coefficients of CO (○), DPA (□), and DPCP (△) on the mole fraction of CO_2 in solution together with the inverse of viscosity (◆) for a mixture of CO_2 and [BMIm][PF_6] from Ref. 14. Blue marks represent [BMIm][NTf_2], green [BMIm][BF_4], and red [BMIm][PF_6], respectively.

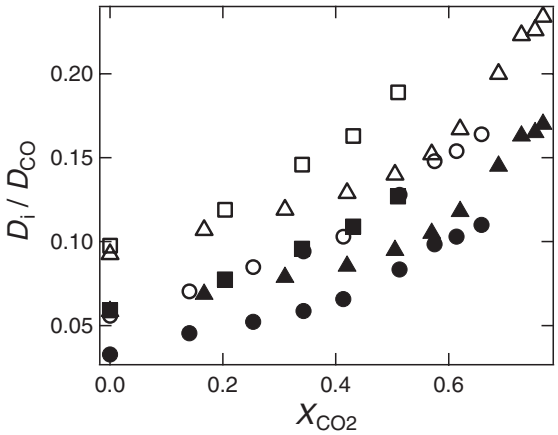

Figure 5. Dependence of the ratio of the diffusion coefficients (filled symbols: D_{DPCP}/D_{CO} and open symbols D_{DPA}/D_{CO}) against the mole fraction of CO_2 in RTILs (●○: [BMIm][PF_6], ▲△: [BMIm][NTf_2], and ■□: [BMIm][BF_4]).

the structure fluctuation. However, as is mentioned later that the variation of the conformer is quite small, and the reason for the larger effect on [BMIm][NTf_2] may be ascribed to another reason such as the molecular symmetry of anion. However, at present we do not have a clear answer.

Pressure Dependence of the Diffusion Coefficients. Tables 3–5 summarize the thermal diffusivity and the translational diffusion coefficients of CO, DPA, and DPCP under various pressures of CO_2 in [BMIm][NTf_2] and [BMIm][BF_4], together with those in [BMIm][PF_6]. As is shown in the tables, the thermal diffusivity of the mixture is insensitive to the CO_2 pressure within the accuracy of our experiments, as observed for the case of [BMIm][PF_6].[16] Figure 4 plots the diffusion coefficients against the mole fraction of CO_2 together with the inverse of the viscosity of the CO_2 mixture of [BMIm][PF_6].[14] As is shown in Figure 4, the translational diffusion coefficients of CO, DPA, and DPCP increase significantly with increasing the mole fraction of CO_2 in solution. According to the Stoke–Einstein (SE) relationship, the diffusion coefficient is inversely proportional to the viscosity (η) and the radius of the solute molecule (r) as

$$D = \frac{k_B T}{C\pi\eta r} \tag{3}$$

where k_B, and T are the Boltzmann constant and the temperature, respectively. The constant C is dependent on the boundary condition of the surface flow (4 for the slip, 6 for the stick boundary condition). As is shown in Figure 4, the diffusion coefficients in the mixture solutions increase with decreasing viscosity of the mixture solution in the case of [BMIm][PF_6] as is predicted by eq 3. Although there is no available information on the viscosity for other RTIL mixtures used here, viscosities of the mixtures are also expected to decrease with increasing CO_2 pressure, since the cation–anion interaction is weakened by the presence of CO_2 as is discussed in the previous section.

However, as mentioned in a previous paper,[16] detailed comparison of the viscosity dependence of different solute molecules reveals that the SE relation does not hold; i.e., the viscosity dependences of D_{DPA} and D_{DPCP} in the CO_2 mixture of [BMIm][PF_6] are much larger than is expected from the SE relation, while the dependence of D_{CO} is small. Similar trends are observed for the CO_2 mixtures of [BMIm][NTf_2] and [BMIm][BF_4]. For example, the diffusion coefficients of the larger molecule (DPA and DPCP) in the CO_2 mixture of [BMIm][NTf_2] at 10 MPa ($X_{CO_2} = 0.73$) are nearly ten times larger than those under ambient conditions, while the diffusion coefficient of the smallest molecule (CO) at 10 MPa is only about 3 times larger than that under ambient conditions. Figure 5 shows the dependence of the ratio D_{DPCP}/D_{CO} on the mole fraction of CO_2. The dependence is somewhat smaller for the CO_2 mixture of [BMIm][NTf_2].

In the previous paper, we have proposed two probable reasons for the size dependence of the solute diffusion. One is the void volume effect produced by the structure composed by cation and anion and the other is the inhomogeneity effect.[16] It has been reported that small molecules like CO can move much faster than the estimation from the SE equation, and this is often ascribed to the voids of RTILs.[2,30] When the solute molecule moves from one void to another, solvent reorganization is subtle and therefore, the friction for the small solute is smaller than the Stokes friction estimated from the solvent viscosity. By dissolving CO_2, the voids are gradually filled with CO_2 molecules and the void effect on the diffusion gradually diminishes and comes to follow the ordinal diffusion mechanism. In this interpretation, the size dependence is ascribed to the extraordinarily fast diffusion of the small solute molecule under ambient conditions. From this point of view, the volume expansion of the mixture may be related to the

change of the ratio of the diffusion coefficients e.g., (D_{DPCP}/D_{CO} and D_{DPA}/D_{CO}) (Figure 5). The ratio is smallest in [BMIm][PF_6] at 0.1 MPa ($X_{CO_2} = 0$). This is probably because the size effect is more significant in the viscous RTILs[2,30] and [BMIm][PF_6] is more viscous (260 mPa s) than other RTILs used here under ambient conditions. As is shown in the figure, the ratio increases with increasing X_{CO_2} and the dependence is moderate in [BMIm][NTf_2]. If we simply calculate the volume for CO_2 in the mixture by subtracting the pure molar volume of RTIL from the volume of the CO_2 mixture of 1 molar RTIL, the CO_2 mixture of [BMIm][NTf_2] gives the largest among the RTILs studied here if compared at the same mole fraction of CO_2 (the volume is ca. 42 $cm^3\,mol^{-1}$ for $X_{CO_2} = 0.3$ in the CO_2 mixture of [BMIm][NTf_2], while it is ca. 28 and 34 $cm^3\,mol^{-1}$ in the CO_2 mixture of [BMIm][PF_6] and [BMIm][BF_4], respectively. These values are calculated by V_r in Tables 3–5 and ρ at 0.1 MPa without CO_2 in Tables 1 and 2). This relatively large space for CO_2 in [BMIm][NTf_2] may be used for the diffusion of the smaller molecule CO, which results in the relatively smaller dependence of D_{DPCP}/D_{CO} and D_{DPA}/D_{CO} against X_{CO_2} in [BMIm][NTf_2] shown in Figure 5. Of course, the variation of the viscosity of the mixture by applying CO_2 will be strongly coupled with the ratio change, which should be discussed in the future.

Before the discussion on the local structure around DPCP by Raman spectroscopic study, we mention the effect of the heterogeneity of RTILs. Several spectroscopic studies have revealed that there is heterogeneity of the solvation in RTILs.[18,37–40] For example, Mandal et al. found that the fluorescence of 2-amino-7-nitrofluorene showed excitation wavelength dependence (red-edge effect) in RTILs,[37] suggesting that the solute molecule is differently solvated in RTILs depending on the local environment. This kind of heterogeneity is suggested to be due to the existence of the polar and nonpolar parts of the cation molecule. If DPCP molecule is solvated by the polar part of the cation and CO molecule is preferentially solvated by the nonpolar part, the solvent effect on the diffusion may be different. It is plausible that the effect of this preference solvation may be reduced by applying CO_2 as mentioned in the previous paper.[16] However, it will be shown in the next section that the molecular interaction between solute and cation or anion is not strongly affected by the presence of CO_2. Further the segregated structure observed for the RTILs with the longer alkyl-chains, which is considered to be a typical example of the structure heterogeneity, is not strongly affected by the presence of CO_2.

Solute–Solvent Interaction Measured by Raman Spectroscopy. Figure 6 shows the Raman spectra around the finger print region of the solution of DPCP in the CO_2 mixture of [BMIm][PF_6]. Almost no shift was detected for the Raman bands assigned to the [BMIm][PF_6] vibrations, and only the Fermi splitting band of the stretching vibration of CO_2 shows an increase of the relative strength with increasing the CO_2 pressure.[12] The inset shows the magnification of the band assigned to the C=C + C=O stretching vibration of DPCP (around 1625 cm^{-1}). It has been shown that this band is a good indicator of the solvent acceptor number (AN).[18] With increasing electrophilicity or Lewis acidity of the solvent, solvent interaction with the oxygen atom of DPCP weakens the

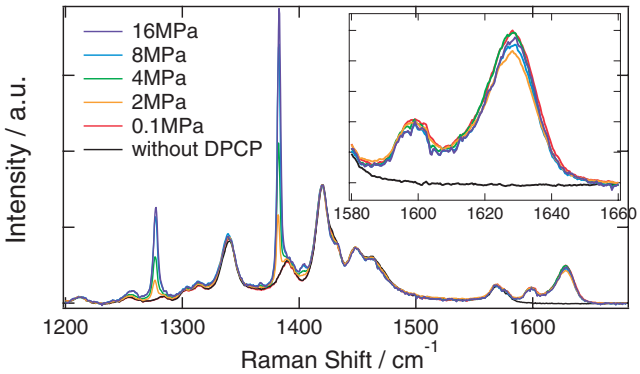

Figure 6. Raman spectra of the DPCP solution of the mixture of CO_2 and [BMIm][PF_6] under various pressures of CO_2. The inset shows the magnification of the region corresponding to the C=C + C=O band of DPCP.

C=O bond, which results in the shift of the Raman band. As is shown in Figure 6, the Raman band of DPCP is almost unchanged with increasing CO_2 pressure, which means that the Lewis acidity of [BMIm][PF_6] is almost unchanged by the presence of CO_2. According to previous studies, the ANs of RTILs are mainly determined by the species of cation, and the present result indicates that the local interaction between cation and DPCP is not strongly affected by the presence of CO_2. The same result was also obtained for the CO_2 mixture of [BMIm][NTf_2]. Therefore the change of the diffusion coefficient of DPCP with an increase of CO_2 may not come from the direct change of the cation–DPCP interaction. The insensitivity of the solvation structure to CO_2 has also been demonstrated by solvatochromic parameters. Fredlake et al. have measured the CO_2 pressure dependence of the absorption spectra of 4-nitroaniline, *N*,*N*-diethyl-4-nitroaniline and Reichardt dye 33 and determined the Kamlet–Taft parameters of π^*, α, and β.[41] According to their results, these parameters are almost insensitive to the presence of CO_2, irrespective of the species of anion which composes the RTILs. Therefore, although the anion–CO_2 interaction is suggested to be stronger than cation–CO_2 by the MD simulations,[6,7,17] the interaction of the organic solute molecule with cation or anion is stronger than the interaction of the solute with CO_2, and the presence of CO_2 does not disturb the local solvation structure.

Figure 7 shows the Raman spectra of [BMIm][NTf_2] around 250 to 450 cm^{-1} region. It is reported that these Raman bands belong to the vibrations of NTf_2^- anion due to the different conformers. In particular two bands around 400 cm^{-1} represent the conformational equilibrium of s-cis and s-trans conformer of the NTf_2 anion.[42] The peak positions and relative strengths of these bands are hardly dependent on the CO_2 pressure, and the conformational equilibrium is not strongly affected by the presence of CO_2. This also suggests that the interaction between CO_2 and anion is not strong enough to affect the conformational structure of anion, although CO_2 molecules are suggested to be preferably solvated by anion molecules in RTILs.

Nanoscale Structure. In this section, we will focus a larger-scale structure of RTILs. Figure 8 shows the SAXS profiles of the mixture of CO_2 and [OMIm][BF_4] under the

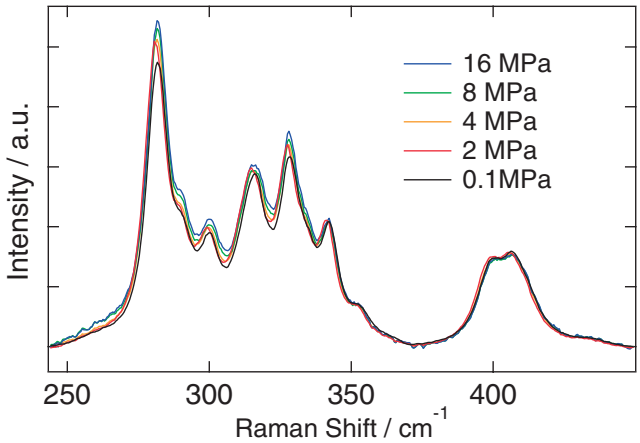

Figure 7. Raman spectra of a CO_2 mixture of [BMIm][NTf_2] under various pressures of CO_2.

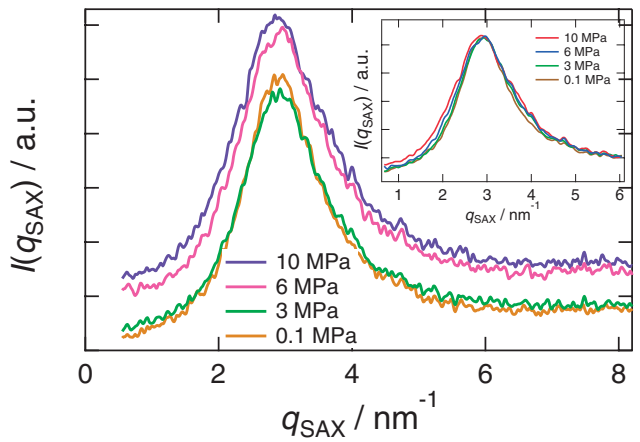

Figure 8. SAXS profiles of the CO_2 mixture of [OMIm][BF_4] under various pressures of CO_2. The inset shows the scaled intensity at each pressure in order to compare the peak position and the band width. The mole fractions of CO_2 (X_{CO_2}) are estimated to be 0.35 (3 MPa), 0.54 (6 MPa), and 0.66 (10 MPa) from Refs. 5 and 43. The relative volume changes of 1 molar [OMIm][BF_4] (V_r) are 1.07 (3 MPa), 1.15 (6 MPa), and 1.21 (12 MPa) from Ref. 3.

several CO_2 pressures. The values of X_{CO_2} and V_r are evaluated by interpolating the values in the literature,[3,43] which are listed in the figure caption. At the highest pressure (10 MPa), X_{CO_2} and V_r are 0.66 and 1.21, respectively. Around $q_{SAX} = 3\,nm^{-1}$ region, a peak is observed as was reported previously, which is assigned to the local ordering of RTILs.[26,27] Here we show the result for the different ionic liquid ([OMIm][BF_4]) from those studied by TG and Raman, because the SAXS profiles of BMIm-cation-based ionic liquids do not show a peak corresponding to the nano-order scaling.[44] Interestingly, the intensity of the SAXS profile increases with increasing the CO_2 pressure and the peak position of the SAXS profile scarcely shifts with increasing the CO_2 pressure. The increase of the SAXS intensity may be correlated with concentration fluctuation and density fluctuation of the solution. The trend is similar to the increase of the density fluctuation of the mixture observed for BMIm-cation-based ionic liquids. However, we will not discuss the intensity change furthermore in this paper, because we cannot deny the possibility that the relative SAXS intensity is affected by the replacement of the high pressure cell from the beamline at each pressure as is mentioned in the experimental procedure. The correction using the absorption of X-rays is naive and more careful experimental procedure will be required to discuss the relative intensity. Hereafter we will concentrate on the SAXS profile around the peak position.

In order to see the peak profile at $q_{SAX} = 3\,nm^{-1}$, the SAXS profiles normalized by the relative intensity at the peak value to the value at $q_{SAX} = 8\,nm^{-1}$ are shown in the inset figure of Figure 8. It is clearly shown that the peak position is almost unchanged with the CO_2 pressure. This means that the size of the structure ordering is not affected by the presence of CO_2. The results seem to be consistent with the prediction by the MD simulation suggesting that the CO_2 molecule is dissolved into the void space.[6,7] On the other hand, the width of the peak increases with increasing the CO_2 pressure, suggesting that the fluctuation of the domain-structure increases. The fluctuation of the nanoscale ordering indicates that the interaction which forms the ordering is disturbed by the dissolved CO_2. It is possible that such disturbance of the interaction may loosen the structure and affect the dynamics properties such as viscosity. Although the present work is for long alkyl-chain RTIL ([OMIm][BF_4]), a similar enhancement of the structure fluctuation may possible for shorter alkyl chain RTILs, because the value of β_S increases by increasing CO_2 pressure as shown in the previous section.

Conclusion

In this paper, we presented the diffusion coefficients of solute molecules dissolved in CO_2 mixtures of [BMIm][NTf_2] and [BMIm][BF_4], together with structural information such as isentropic compressibility, the vibrational spectra of the mixture solution, and the SAXS profile. The CO_2 pressure dependence of the diffusion coefficients of CO, DPA, and DPCP were consistent with previous results for CO_2 mixtures of [BMIm][PF_6]. The CO_2 effect on the isentropic compressibility was more significant for [BMIm][NTf_2] than that for [BMIm][PF_6] and [BMIm][BF_4]. According to the SAXS results, the length of the nanoscaling of [OMIm][BF_4] was not affected by the presence of CO_2, although an increase of the fluctuation of the nanoscale ordering was observed. By summarizing these observations, the enhanced translational diffusion coefficients are mainly due to the change of the solution viscosity. The variation of the viscosity comes from the enhanced fluctuation of the bulk structure as is represented by the larger isentropic compressibility. The solute size dependence of the diffusion coefficients is suggested to be related with the structure of RTILs. Raman spectra of the mixture suggested that the presence of CO_2 does not strongly affect the solvation structure on DPCP as observed for the other dye molecules used for the solvatochromic probes.[41] By the present study, however, we did not see the dynamics related the local environment of the solute molecule. It is an interesting issue whether or not the local dynamics are affected by the presence of CO_2. In order to see this point, we are now evaluating the solvation dynamics of the mixture solution, and the results will appear in the near future.

This work is supported by the Grant-in-Aid for Scientific Research (No. 17073012) from the Ministry of Education, Culture, Sports, Science and Technology. This work is also partially supported by Core Stage Program from Kyoto University. We are grateful to the approval of Photon Factory Advisory Committee (PAC) (Proposal No. 2009G518) at High Energy Accelerator Research Organization (KEK) for the SAXS measurements.

References

1 L. A. Blanchard, D. Hancu, E. J. Beckman, J. F. Brennecke, *Nature* **1999**, *399*, 28.

2 See, e.g.: J. Huang, T. Rüther, *Aust. J. Chem.* **2009**, *62*, 298, and references cited therein.

3 L. A. Blanchard, Z. Gu, J. F. Brennecke, *J. Phys. Chem. B* **2001**, *105*, 2437.

4 J. L. Anthony, E. J. Maginn, J. F. Brennecke, *J. Phys. Chem. B* **2002**, *106*, 7315.

5 S. N. V. K. Aki, B. R. Mellein, E. M. Saurer, J. F. Brennecke, *J. Phys. Chem. B* **2004**, *108*, 20355.

6 C. Cadena, J. L. Anthony, J. K. Shah, T. I. Morrow, J. F. Brennecke, E. J. Maginn, *J. Am. Chem. Soc.* **2004**, *126*, 5300.

7 X. Huang, C. J. Margulis, Y. Li, B. J. Berne, *J. Am. Chem. Soc.* **2005**, *127*, 17842.

8 B. L. Bhargava, S. Balasubramanian, *J. Phys. Chem. B* **2007**, *111*, 4477.

9 M. Kanakubo, T. Umecky, Y. Hiejima, T. Aizawa, H. Nanjo, Y. Kameda, *J. Phys. Chem. B* **2005**, *109*, 13847.

10 S. G. Kazarian, B. J. Briscoe, T. Welton, *Chem. Commun.* **2000**, 2047.

11 T. Seki, J.-D. Grunwaldt, A. Baiker, *J. Phys. Chem. B* **2009**, *113*, 114.

12 J.-M. Andanson, F. Jutz, A. Baiker, *J. Phys. Chem. B* **2009**, *113*, 10249.

13 T. Makino, *J. Phys.: Conf. Ser.* **2010**, *215*, 012068.

14 Z. Liu, W. Wu, B. Han, Z. Dong, G. Zhao, J. Wang, T. Jiang, G. Yang, *Chem.—Eur. J.* **2003**, *9*, 3897.

15 M. Kanakubo, T. Umecky, T. Aizawa, Y. Ikushima, *Electrochemistry* **2004**, *72*, 703.

16 M. Demizu, M. Terazima, Y. Kimura, *Anal. Sci.* **2008**, *24*, 1329.

17 B. L. Bhargava, A. C. Krishna, S. Balasubramanian, *AIChE J.* **2008**, *54*, 2971.

18 T. Fujisawa, M. Fukuda, M. Terazima, Y. Kimura, *J. Phys. Chem. A* **2006**, *110*, 6164.

19 H. Hamaguchi, R. Ozawa, *Adv. Chem. Phys.* **2005**, *131*, 85.

20 K. Iwata, H. Okajima, S. Saha, H. Hamaguchi, *Acc. Chem. Res.* **2007**, *40*, 1174.

21 S. Shigeto, H. Hamaguchi, *Chem. Phys. Lett.* **2006**, *427*, 329.

22 Y. Wang, G. A. Voth, *J. Am. Chem. Soc.* **2005**, *127*, 12192.

23 Y. Wang, G. A. Voth, *J. Phys. Chem. B* **2006**, *110*, 18601.

24 J. N. A. Canongia Lopes, A. A. H. Pádua, *J. Phys. Chem. B* **2006**, *110*, 3330.

25 Z. Hu, C. J. Margulis, *Proc. Natl. Acad. Sci. U.S.A.* **2006**, *103*, 831.

26 A. Triolo, O. Russina, H.-J. Bleif, E. Di Cola, *J. Phys. Chem. B* **2007**, *111*, 4641.

27 A. Triolo, O. Russina, B. Fazio, G. B. Appetecchi, M. Carewska, S. Passerini, *J. Chem. Phys.* **2009**, *130*, 164521.

28 T. Yamaguchi, Y. Kimura, N. Hirota, *J. Phys. Chem. A* **1997**, *101*, 9050.

29 *Ionic Liquids in Synthesis*, 2nd ed., ed. by P. Wasserscheid, T. Welton, Wiley-VCH Verlag GmbH & Co. KGaA, Weinheim, **2008**.

30 Y. Nishiyama, M. Fukuda, M. Terazima, Y. Kimura, *J. Chem. Phys.* **2008**, *128*, 164514.

31 T. Fujisawa, M. Terazima, Y. Kimura, *J. Phys. Chem. A* **2008**, *112*, 5515.

32 M. Harada, K. Kuramitsu, Y. Kimura, K. Saijo, *Colloids Surf., A* **2008**, *327*, 21.

33 R. G. de Azevedo, J. M. S. S. Esperança, J. Szydlowski, Z. P. Visak, P. F. Pires, H. J. R. Guedes, L. P. N. Rebelo, *J. Chem. Thermodyn.* **2005**, *37*, 888.

34 R. G. de Azevedo, J. M. S. S. Esperança, V. Najdanovic-Visak, Z. P. Visak, H. J. R. Guedes, M. N. da Ponte, L. P. N. Rebelo, *J. Chem. Eng. Data* **2005**, *50*, 997.

35 M. Fukuda, M. Terazima, Y. Kimura, *J. Chem. Phys.* **2008**, *128*, 114508.

36 M. Herstedt, M. Smirnov, P. Johansson, M. Chami, J. Grondin, L. Servant, J. C. Lassègues, *J. Raman Spectrosc.* **2005**, *36*, 762.

37 P. K. Mandal, M. Sarkar, A. Samanta, *J. Phys. Chem. A* **2004**, *108*, 9048.

38 A. Paul, P. K. Mandal, A. Samanta, *J. Phys. Chem. B* **2005**, *109*, 9148.

39 H. Jin, X. Li, M. Maroncelli, *J. Phys. Chem. B* **2007**, *111*, 13473.

40 Y. Kimura, T. Hamamoto, M. Terazima, *J. Phys. Chem. A* **2007**, *111*, 7081.

41 C. P. Fredlake, M. J. Muldoon, S. N. V. K. Aki, T. Welton, J. F. Brennecke, *Phys. Chem. Chem. Phys.* **2004**, *6*, 3280.

42 J. C. Lassègues, J. Grondin, R. Holomb, P. Johansson, *J. Raman Spectrosc.* **2007**, *38*, 551.

43 K. I. Gutkowski, A. Shariati, C. J. Peters, *J. Supercrit. Fluids* **2006**, *39*, 187.

44 Although we tried to see the difference of the SAXS profiles under CO_2 pressure for [BMIm][BF_4], we could not see a meaningful difference in the profile under different pressure, since they did not show any peaks around the corresponding position.